JOURNAL OF GEOPHYSICAL RESEARCH, VOL. 95, NO. B10, PAGES 15,817–15,827, SEPTEMBER 10, 1990

Phase Relations of Aluminum-Undepleted and Aluminum-Depleted Komatiites at Pressures of 4-12 GPa

KEJIAN WEI, REIDAR G. TRØNNES, AND CHRISTOPHER M. SCARFE[1]

C. M. Scarfe Laboratory of Experimental Petrology, Department of Geology and Institute of Earth and Planetary Physics. University of Alberta, Edmonton, Canada

The anhydrous phase relations of natural Al-undepleted komatiite (AUK) with 25% MgO and Al-depleted komatiite (ADK) with 32% MgO have been investigated in the pressure range from 4 to 12 GPa, using samples from Munro Township, Ontario, and the Barberton Mountains, South Africa. The experiments were carried out with graphite or molybdenum capsules in 18-mm octahedral pressure cells in a uniaxial split-sphere multianvil apparatus. The thermal gradient within the stepped resistance heaters of graphite and lanthanum chromite was about 50°C/mm. For both compositions, the liquidus phase is olivine at low pressure (up to 5.6 and 9.6 GPa for the AUK and ADK, respectively) and garnet at high pressure. Pyroxene is the only liquidus phase in an intermediate pressure range for the ADK (9.6–11.5 GPa) and reaches the liquidus at a multiple saturation point with olivine and garnet at 5.6 GPa pressure for the AUK. The subsolidus assemblage consists of olivine, pyroxene, and garnet in the entire pressure range for both of the compositions. The pyroxenes have variable CaO contents, and most of them are subcalcic clinopyroxenes, but minor amounts of orthopyroxene have been observed in some of the run products. If AUK and ADK compositions represent near primary magmas, the melt separation most likely occurred at pressures corresponding to the three phase saturation point at 5.6 GPa for AUK and one of the two cosaturation points (olivine-pyroxene at 9.6 GPa and pyroxene-garnet at 11.6 GPa) for the ADK. The low Ca/Al ratio of the AUK requires a nearly complete melting of garnet. The high Ca/Al ratio of the ADK indicates that garnet was a residual phase at the time of melt separation, or that the mantle source experienced some premelting or synmelting garnet fractionation. The clinopyroxene liquidus interval between 9.6 and 11.6 GPa excludes the coexistence of garnet and olivine in the residue, and the following alternative petrogenetic models are suggested for the ADK: 1. The initial melt was more magnesian than the source peridotite, and the melting progressed to the stage of disappearance of the residual olivine. The melting progressed further along the pyroxene-garnet cotectic before melt separation. 2. Garnet fractionation took place from an ascending and partially molten peridotite diapir. Further melting of the upper portion of the diapir produced a melt that was less magnesian than the source diapir. This could lead to total melt consumption of any remaining residual garnet, and further melting could proceed along the olivine-pyroxene cotectic before final melt separation.

INTRODUCTION

The widespread occurrence of komatiites in Archean greenstone belts [*Arndt*, 1979] indicates that ultramafic magmatism played an important role in the chemical differentiation of the Archean mantle. Information about their petrogenesis is therefore essential for our understanding of the geochemical and geophysical characteristics of the Archean mantle.

Various models have been proposed for the origin of komatiites. *Viljoen and Viljoen* [1969*a*, *b*], *Cawthorn and Strong* [1974], *Green* [1975], *Sun and Nesbitt* [1978], *Nesbitt et al.* [1979], and *Jahn et al.* [1980], for instance, suggested that high magnesium liquids were generated by high degrees (up to 70%) of partial melting of a mantle source at relatively shallow level. *Arndt* [1977] and *Arth et al.* [1977] proposed a sequential melting model in which an ultrabasic magma was formed by further melting of a refractory residue containing small amounts of trapped basic liquid after an initial basic magma separation. The model proposed by *Bickle et al.* [1977] suggests that komatiites are liquids that were separated from the source (dunite, harzburgite) and later assimilated a crystalline fraction during ascent. More recent studies suggest low degrees of pseudoinvariant melting at very high pressures. During their melting experiments, *Takahashi and Scarfe* [1985], *Scarfe and Takahashi* [1986], and *Takahashi* [1986] observed that liquids formed by partial melting of peridotite at its solidus become more magnesian with increasing pressure and that a komatiitic liquid was produced at 5-7 GPa coexisting with residual olivine, clinopyroxene, and garnet. *Herzberg and O'Hara* [1985] and *Herzberg and Ohtani* [1988] examined the locations of komatiites in liquidus projection diagrams and noticed that komatiites are distributed near the experimentally determined pseudoinvariant melting points of peridotite. They suggested, accordingly, that komatiites could have been formed by pseudoinvariant melting (olivine + pyroxene + garnet + liquid).

Nesbitt et al. [1979] divided komatiites into aluminum undepleted komatiites (AUK) and aluminum depleted komatiites (ADK). The chemical characteristics of the different types are shown in Table 1 and Figure 1. The compositional difference between AUK and ADK (e.g., higher Ca/Al and Gd/Yb in ADK than in AUK) has been explained by varying degrees of garnet and clinopyroxene involvement during melting or later fractionation. *Cawthorn and Strong* [1974] suggested that the contrasting compositions are due to the ratio of clinopyroxene/garnet in the original peridotitic source. *Arndt* [1977], *Arndt et al.* [1977], and *Arth et al.* [1977], however, argued that the chemical signature of komatiites is mainly a function of the relative proportion of

[1] Deceased, July 20, 1988.

Paper number 90JB00311.
0148-0227/90/90JB-00311$05.00

TABLE 1. Compositions of Starting Materials Compared to Typical Komatiites, Peridotites and C1 Chondrite

	M620	HSS-15	AUK	ADK	Pyrolite	KLB-1	C1
SiO_2	45.60	46.77	45.90	47.16	45.20	44.48	33.64
TiO_2	0.40	0.33	0.41	0.38	0.71	0.16	0.11
Al_2O_3	7.95	3.42	7.97	4.09	3.54	3.59	2.42
FeO*	12.66	11.26	11.07	12.01	8.47	8.10	36.20
MnO	0.20	0.19	0.21	0.20	0.14	0.12	0.38
MgO	25.00	31.51	26.38	27.97	37.48	39.22	24.23
CaO	7.60	5.67	7.74	6.61	3.08	3.44	1.92
Na_2O	0.01	0.12	0.43	0.37	0.57	0.30	1.00
K_2O	0.02	0.08	0.09	0.04	0.13	0.02	0.10
Mg #	77.9	83.3	80.9	80.6	88.8	89.6	54.4
CaO/Al_2O_3	0.96	1.66	0.97	1.62	0.87	0.96	0.79
Al_2O_3/TiO_2	19.9	10.4	19.4	10.8	4.99	22.4	22.0
$(La/Sm)_n$			0.4-0.8	~1			1
$(Gd/Yb)_n$			~1	~1.43			1
Zr/Y			2.5	2.8-4.6			2.5
Ti/Zr			110	100			111
Ti/Sc			79	110			75

M620, Al-undepleted komatiite from Munro Township, Ontario [*Arndt and Nesbitt* , 1984]; HSS-15, Al-depleted komatiite from Barberton, South Africa [*Smith and Erlank*, 1982]; AUK, average of 22 Al-undepleted komatiites from *Nesbitt et al.*[1979], *Arndt and Nesbitt* [1984], *Cattell and Arndt* [1987] and *Nisbet et al.* [1987]; ADK, average of 18 Al-depleted komatiites from *Nesbitt et al.* [1979] and *Smith and Erlank* [1982]; trace element ratios for ADK and AUK from *Nesbitt et al.* [1982]; Pyrolite, model fertile mantle composition from *Ringwood* [1966]; KLB-1, sinel lherzolite [*Takahashi*, 1986]; C1, average C1 chondrite, oxides calculated from the atomic abundances of *Anders and Grevesse* [1989].

The analyses are normalized to 100% on a volatile free basis; Mg #=[Mg/(Mg+Fe)] x100; *n*, normalized to chondritic abundances.

*Total iron as FeO.

garnet and clinopyroxene retained in their residue. On the other hand, *Green* [1975], *Sun and Nesbitt* [1978], and *Nesbitt et al.* [1979] suggested that the removal of garnet from the source could explain the depletion of aluminum. More recently, *Ohtani* [1984] and *Herzberg and Ohtani* [1988] proposed that Al-undepleted komatiites and Al-depleted komatiites were formed at different depths.

Most of the previous studies of the origin of komatiites have concentrated on the geochemistry (major elements, trace elements, and isotopic ratios). These investigations have placed some constraints on the chemical characteristics of the sources of komatiites, but the depth and thermal condition of komatiite derivation as well as the residual mineral assemblage in the source are still uncertain. Knowledge of the phase relationships of komatiites is essential to understand the origin of the primary magmas of such rocks. Assuming that the primary magma was in equilibrium with its residual source before separation, an examination of the phase relationships of komatiites with compositions near the primary magma at various pressures can provide information about: (1) the residual mineral assemblage from which the magma was extracted; (2) the pressure and temperature under which the magma could coexist with the residual minerals in the source; and (3) the partitioning of elements between residual phases and the magma.

We have studied the phase relationships of komatiites at pressures above 4 GPa for several reasons. A few experimental studies [*Green et al.*, 1975; *Arndt*, 1976; *Bickle et al.*, 1977] have already been done below 4 GPa, and only olivine was found as liquidus phase in the investigated pressure range. The studies by *Ohtani* [1984], *Takahashi and Scarfe* [1985], *Herzberg and Ohtani* [1988], and *Herzberg et al.* [this issue] indicate that understanding the phase relationships of Al-undepleted and Al-depleted komatiites at very high pressures (> 4 GPa) is important for the interpretation of the origin of komatiites.

STARTING MATERIAL

The selection of starting materials was aimed at finding samples with compositions as close as possible to assumed primary melt composition. Textural criteria in the form of spinifex texture and chilled margins of pillow lavas or flow top breccias was used to choose quenched liquid material. The compositions of the two chosen samples are listed in Table 1.

The sample M620 [*Arndt and Nesbitt*, 1984] was collected from a spinifex-textured komatiitic lava in Munro Township, Ontario. This sample contains 25 wt % MgO and has Al/Ti and Ca/Al ratios close to the average of Al-undepleted komatiite (Table 1). The sample displays typical spinifex texture with skeletal blades of olivine pseudomorphs (10-15 mm long but only 0.3-1 mm wide) randomly oriented in a matrix of fine skeletal clinopyroxene and devitrified glass. The olivine has been entirely replaced by fine grained hydrous minerals, but most clinopyroxenes remain fresh. Detailed descriptions of field geology, petrology, and geochemistry of the komatiites from this area have been given by *Pyke et al.* [1973], *Arndt et al.* [1977], *Arth et al.* [1977], *Arndt and Nesbitt* [1982] and *Arndt and Nesbitt* [1984]. A Sm-Nd age of 2.6 Ga for komatiites from Munro Township was provided by *Zindler* [1982]. Although M620 has not been investigated experimentally, a sample (SA 3091) of composition similar to M620 from the same area was used in the experiments by *Arndt* [1976].

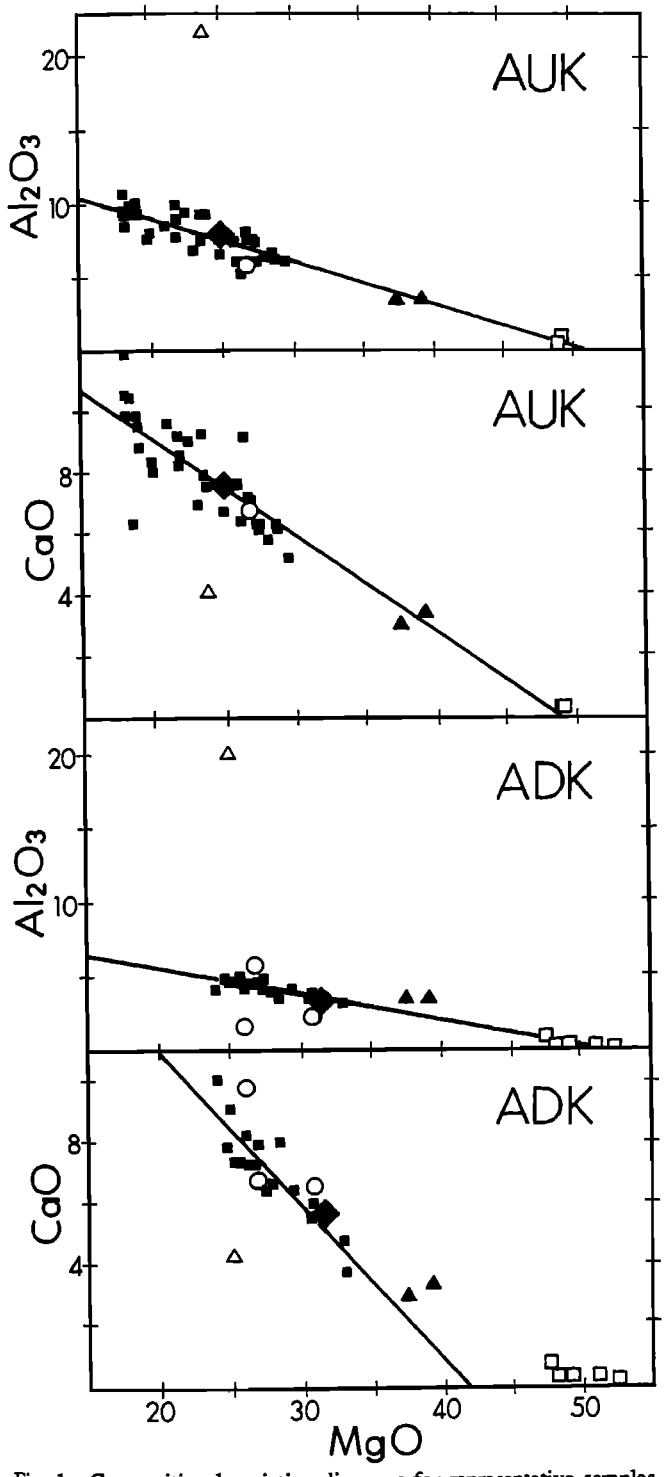

Fig. 1. Compositional variation diagrams for representative samples of Al-undepleted komatiites (AUK) and Al-depleted komatiites (ADK). Solid squares are komatiites; (top) AUK, samples from Munro Township, Ontario [*Arndt andNesbitt*, 1984; *Arndt et al.*, 1977; *Nesbitt et al.*, 1979], Newton Township, Ontario [*Cattell and Arndt*, 1987], Belingwe greenstone belt, Zimbabwe [*Nisbet et al.*, 1987]; (bottom) ADK, samples from Barberton Mountain Land, South Africa [*Nesbitt et al.*, 1979; *Smith and Erlank*, 1982]. Solid diamonds are starting material compositions (Table 1); AUK: M620, ADK: HSS-15. Solid triangles are peridotite compositions (Table 1); pyrolite and KLB-1. Open squares are liquidus olivine compositions (Table 3); AUK: run 138 and 260, ADK: runs 138, 135, 168, 156, and 247. Open circles are liquidus clinopyroxene compositions (see Table 4); AUK: run 260, ADK: runs 38, 247, and 275. Open triangles are liquidus garnet compositions (Table 4); AUK: run 247, ADK: run 242. The lines are least squares regression fit to the komatiite compositions only.

The sample HSS-15 [*Smith and Erlank*, 1982; H. S. Smith, personal communication, 1988] was collected from a chilled margin of a pillow lava or flow top breccia in the Barberton Mountain Land of South Africa. The chemical analyses (Table 1) show that this sample contains 31.5 wt % MgO and has Ca/Al and Al/Ti ratios close to the average of Al-depleted komatiites. HSS-15 is aphanitic with less than 0.4-mm microphenocrysts of serpentine pseudomorphs of olivine. The geology of Barberton Mountain Land was described by *Anhaeusser et al.* [1968], *Viljoen and Viljoen* [1969*a*, *b*, *c*], *Anhaeusser* [1973, 1978], *Williams and Furnell* [1979], and *Viljoen et al.* [1982], and detailed petrological and geochemical accounts of the komatiites were provided by *Nesbitt et al.* [1979], *Jahn et al.* [1982], and *Smith and Erlank* [1982]. Sm-Nd ages of about 3.6 Ga were provided by *Hamilton et al.* [1979] and *Jahn et al.* [1982]. A sample (J49) from same area was used in the experiments by *Green et al.* [1975].

Experimental Procedures

All experiments were performed in a 2000-t uniaxial split sphere apparatus [see *Ito et al.*, 1984] at the University of Alberta. A semisintered MgO/5% Cr_2O_3 octahedron was used as pressure medium between eight cubic tungsten carbide anvils (32.5-mm side lengths) with truncated corners (11-mm truncation edge).

The furnace assemblies are shown in Figure 2. The ZrO_2 sleeve is a thermal insulator and, together with the Cr_2O_3 of the pressure medium, improves the efficiency of the graphite or $LaCrO_3$ heaters. Graphite heaters were used in most of the experiments below 7 GPa. At the highest pressures and temperatures used in this study, however, rapid kinetics of the transition of graphite to diamond prevent the use of graphite heaters. $LaCrO_3$, with its temperature dependent resistance [*Takahashi*, 1986] and thermal insulating capacity, provides a heater with slightly lower power consumption and lower thermal gradient than a graphite heater.

Graphite sample containers were used for experiments below 9 GPa, and molybdenum capsules were used for most runs above that pressure in order to prevent diamond formation. No metallic iron or iron-molybdenum alloy was observed in our run products, and no iron loss to the molybdenum capsules was detected by electron microprobe analyses. Small amounts of Mo were detected in the quenched liquid portion of the run products from the Mo capsules.

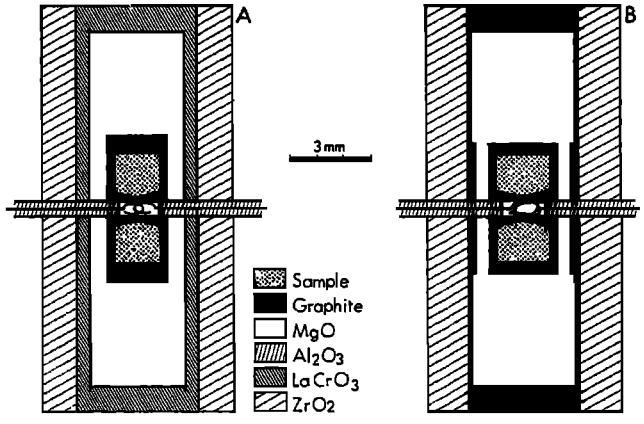

Fig. 2. Cross section of the furnace assemblies. *a*: Simple cylindrial furnace, *b*: Sectioned furnace. Some experiments were also carried out using simple cylindrical graphite heaters and sectioned $LaCrO_3$ heaters.

The sample pressure was calibrated against the load tonnage by using the following transitions: (1) at room temperature, Bi(I-II) at 2.55 GPa [*Hall*, 1971] and Bi(V-VI) at 7.7 GPa [*Homan*, 1975]; (2) at 1000°C, Fe_2SiO_4 (α - γ) at 5.3 GPa [*Yagi et al.*, 1987] and coesite-stishovite at 9.4 GPa [*Suito*, 1977]; (3) at 1500°C and 2000°C, quartz-coesite at 3.6 and 4.2 Gpa, respectively [*Boyd and England*, 1960; *Mirwald and Massonne*, 1980].

Because the shift of the calibration curve between 1000°C and 2000°C does not exceed the uncertainty of the calibration, run pressures were measured based on the pressure calibration at 1000°C. The accuracy and precision of the sample pressure are estimated to be ± 0.2 GPa.

The temperature was monitored with a W3%Re-W25%Re thermocouple that was diametrically inserted through the center of the furnace and electrically insulated from the heater by alumina sleeves (see Figure 2). No correction for the effect of pressure on the thermocouple emf was made. Our recorded temperatures may therefore be somewhat lower than the real temperatures in the hot end of the sample capsules (see discussions by *Getting and Kennedy* [1970] and *Herzberg et al.*, [this issue] and below). Using a programmable controller, the temperature could be controlled to within ± 5°C.

Each sample was ground in an agate mortar under alcohol until the grain size was less than 5-10 μm. The pulverized samples were fired at 1100°C in Ar atmosphere and stored in an oven at 110°C.

Approximatly 10-20 mg fired powder was loaded in a capsule that was then covered with a lid. Two capsules were placed in the internal graphite resistance furnace and insulated from the furnace with MgO sleeves and spacers. The whole assembly (Figure 2) installed in the MgO-Cr_2O_3 octahedron was fired at 1000-1100°C in Ar atmosphere for 1 hour in order to dehydrate all of the parts completely. The assembly was subsequently installed between the tungsten carbide anvils, and the inner anvil configuration was loaded in the space between the outer split-sphere anvils.

The sample pressure was increased to the run pressure by 0.1-0.2 GPa/min, and the temperature was then raised by 100°C/min to the desired value. The run durations are given in

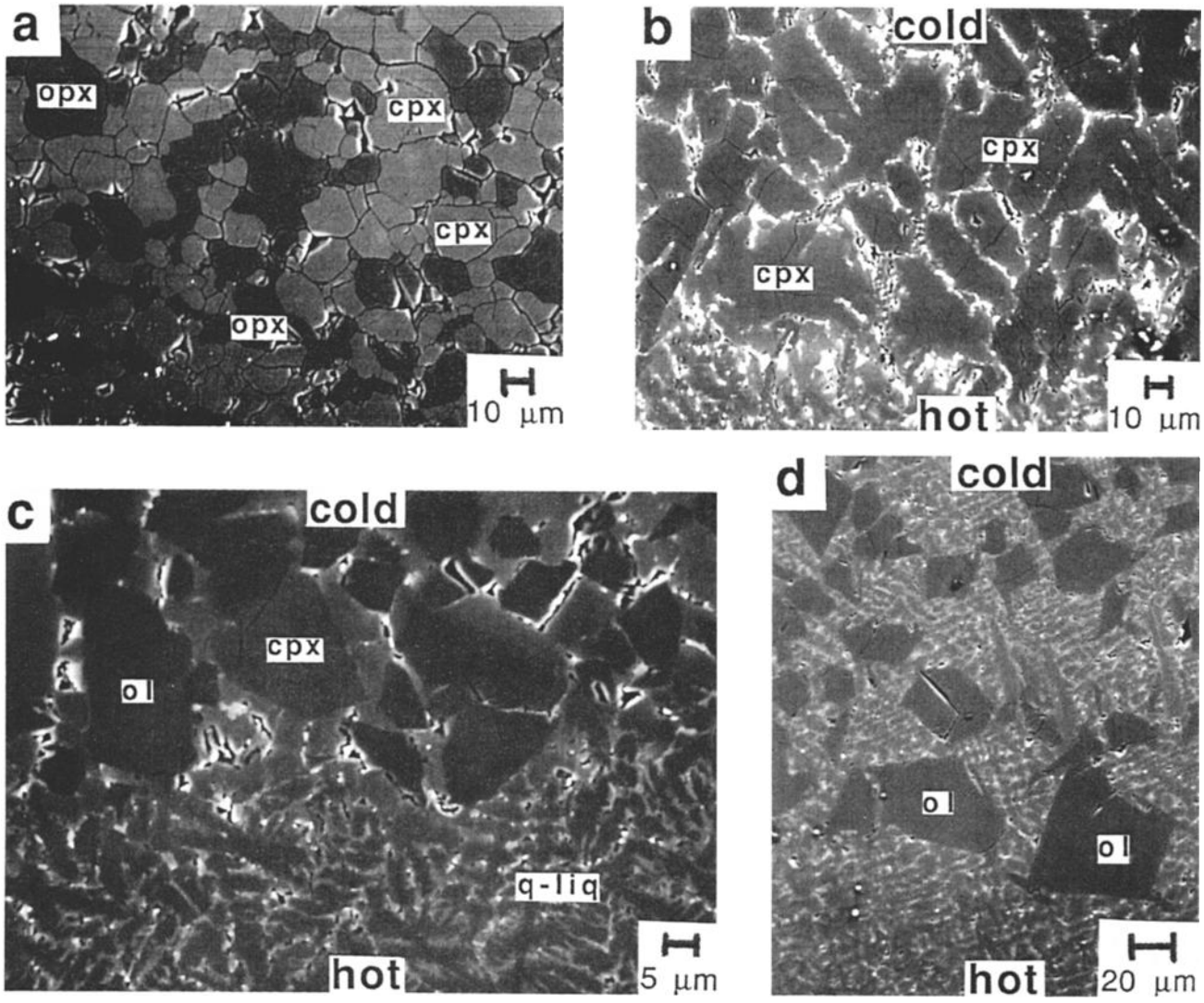

Fig. 3. Back scattered electron SEM photomicrographs of run products. (*a*) Run 245 (not in Table 2), enstatite-diopside mixture held at 7 GPa and 1500°C for 210 min, using a sectioned graphite furnace: equilibrium intergowth texture of orthopyroxene (opx) and clinopyroxene (cpx). (*b*) Run 275, HSS-15: coarse, unzoned clinopyroxenes (cpx) in equilibrium with quenched liquid (q-liq). (*c*) Run 260, M620: coarse, euhedral, and unzoned olivines (ol) and clinopyroxenes (cpx) coexisting with quenched liquid (q-liq). (*d*) Run 156, HSS-15: coarse, euhedral, and unzoned liquidus olivines.

Table 2. The experiments were quenched by turning off the power and the quench time (from run temperature to 400°C) was 2-3 s.

The phases in the run charges were identified by optical microscopy and back scattered electron imaging at the University of Alberta. Selected liquidus phases were analyzed by electron microprobe at the University of Calgary, using 15 kV acceleration voltage and 10-15 mA beam current. The counting time was 20 seconds on peaks and background. The major elements (Si, Ti, Al, Mn, Fe, Mg, Ca, and Na) were measured simultaneously by eight wavelength dispersive spectrometers. Data reduction and correction were made with the *Bence and Albee* [1968] correction scheme, with modification of *Albee and Ray* [1970]. The analytical accuracy and precision (one standard deviation) are ±1.5% of the amount present for oxides comprising more than 5%, ±2-30% for oxides in the 1-5% range and ±3-50% for oxides comprising less than 1% of the analysis.

Temperature Distribution Within the Furnace

Figure 2 shows the two different types of heaters used in this study: a simple cylindrical heater of $LaCrO_3$ (Figure 2*a*) and a sectioned heater of graphite (Figure 2*b*). Some of the experiments were also performed with simple cylindrical graphite heaters or with sectioned $LaCrO_3$ heaters. *Takahashi et al.* [1982] found a thermal gradient of about 200°C/mm along the axis of a simple cylindrical heater. Such a large thermal gradient may provide useful information on the near liquidus and near solidus phase relations in single experimental charges, but it clearly causes a large temperature uncertainty.

The sectioned heater (Figure 2*b*, see also *Fujii et al.* [1989]) was used in 24 of the 28 experiments in order to to reduce the thermal gradient. The effect of this type of heater is similar to that produced by a tapered heater [*Kushiro*, 1976; *Takahashi et al.*, 1982]. Two experiments were carried out with sectioned graphite heaters to map the temperature distribution within the sample capsules, using the two-pyroxene thermometer method described by *Takahashi et al.* [1982]. A mixture of crystalline enstatite and diopside was equilibrated at 5 and 7 GPa and 1500°C (thermocouple reading) for 140 and 210 min, respectively, and the compositions of the coexisting pyroxenes were measured at different locations throughout the samples. Figure 3a shows one of the run products comprising an equilibrium texture intergrowth between orthopyroxene and clinopyroxene. The spatial distribution of K_d (=$(1\text{-Ca})^{cpx}/(1\text{-Ca})^{opx}$) values and corresponding temperatures according to the *Nickel et al.* [1985] thermometer are plotted in Figure 4. The variation of the K_d within 1 mm of the hot end of the capsule ranges from 0.28 to 0.46 and the temperature variation within the same area is about 50°C. The temperature uncertainty inherent in the thermometer is probably at least ±25°C [*Nickel et al.*, 1985]. Independent experiments with a very similar furnace design and two axial thermocouple pairs shows that the axial thermal gradient is less than 10°C/mm near the center of the furnace (M. Kanzaki, University of Alberta, personal communication, 1989). The replacement of graphite by $LaCrO_3$ as heater material seems to lower the thermal gradient slightly.

The thermocouple reading is 50-100°C lower than the thermometer values (Figure 4). This may be due to a combination of the pressure effect on thermocouple emf and local temperature perturbations related to the resistance pattern of the heater in the area of thermocouple penetration [*Herzberg et al.*, this issue]. It is also possible that the thermocouple with sleeves represents an avenue for elevated heat radiation from the furnace.

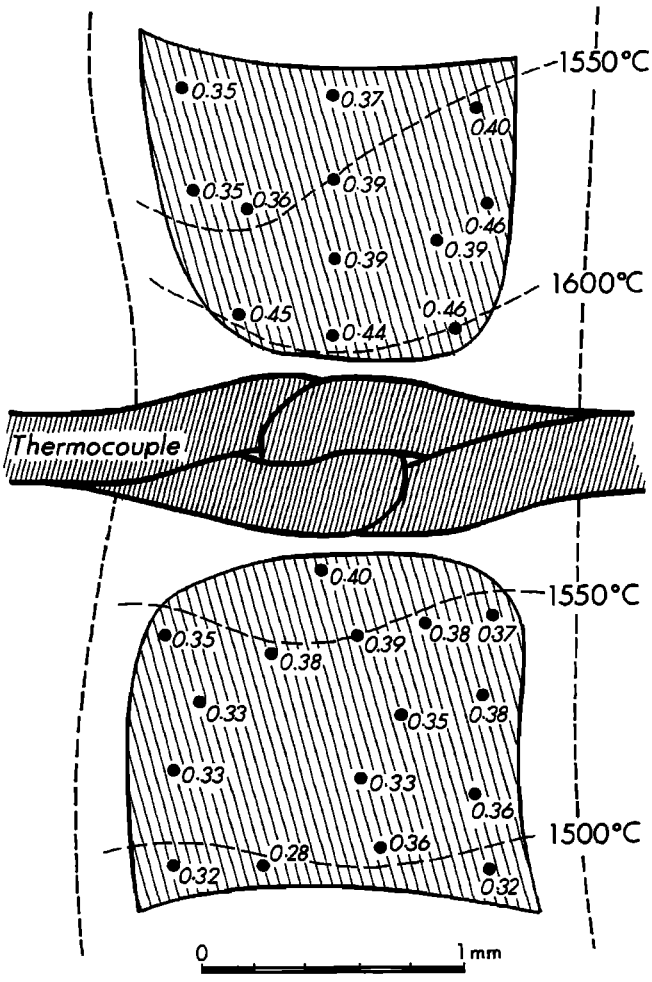

Fig. 4. Temperature distribution within two-pyroxene charges from an experiment at 1500°C (thermocouple reading) and 7 GPa using a sectioned graphite heater (Figure 3*a*). The numbers show the locations of two coexisting pyroxenes and their K_d $[(1\text{-}X_{Ca})^{cpx}/(1\text{-}X_{Ca})^{opx}]$. Light stippled lines indicate temperature contours, and heavy stippled lines are the outside walls of the graphite capsules. See text and Figure 3*a* for further explainations.

In spite of the low thermal gradient in the sectioned heaters, almost all of the run products from suprasolidus experiments show an increasing proportion of melt towards the center of the furnace (Figures 3*b*, 3*c*, and 3*d*). The distribution of melt (quenched crystals) and equilibrium crystals is also independent of whether the sample capsule was above or below the central hot spot, indicating that gravitational separation is not important.

Experimental Results

The phase assemblages listed in Table 2 represent the coexisting phases observed within 0.4 and 0.10 mm of the hot end of the capsules for sectioned heaters and simple cylindrical heaters, respectively. In these portions of the samples the temperature drop from the hot spot is less than 25°C. The run durations, mostly of 5-30 minutes (Table 2), were sufficient to produce large (>20 mm), unzoned and composionally homogeneous crystals within the liquidus-solidus interval.

TABLE 2. Experimental Conditions and Results

Run #	p, GPa	T,* °C	Time, min	Heater	Container	Results	
						AUK(M620)	ADK(HSS-15)
206	4.0	1600	25	B	C	ol+px+ga	ol+px+ga
202	4.0	1650	65	B	C	ol+px+ga+l	ol+px+ga
138	4.0	1700	5	A	C	ol+px+l	ol+px+l
234	4.0	1780	10	B	C	l	l
212	5.0	1700	60	B	C	ol+px+ga+l	ol+px+ga+l
236	5.0	1750	10	B	C	ol+px+l	ol+px+l
135	5.0	1770	5	A	C	ol+l	ol+l
218	5.0	1800	5	B	C	l	l
260	5.5	1780	5	B	C	ol+px+l	
569	5.7	1800	5	A	C	ga+l	
197	6.0	1700	26	B	C	ol+px+ga	ol+px+ga
220	6.0	1750	30	B	C	ol+px+ga+l	ol+px+ga+l
168	6.0	1800	10	B	C	px+ga+l	ol+l
189	6.0	1820	10	B	C		ol+l
192	6.0	1850	20	B	C	l	l
225	7.0	1750	13	B	C	ol+px+ga+l	ol+px+ga
136	7.0	1780	4	A	C	ol+px+ga+l	ol+px+ga+l
270	7.0	1810	5	B	C	px+ga+l	
156	7.0	1830	7	B	C	ga+l	ol+l
127	7.0	1850	1.5	A	C	l	l
227	9.0	1790	8	B	Mo	ol+px+ga	ol+px+ga
244	9.0	1820	5	B	Mo	ol+px+ga+l	ol+px+ga+l
263	9.0	1835	5	B	Mo	cpx+ga+l	
152	9.0	1860	6	B	C	ga+l	ol+l
257	10.0	1800	6	B	Mo	ol+px+ga+l	ol+px+ga
247	10.0	1860	5	B	Mo	ga+l	ol+px+l
275	11.0	1875	4	B	Mo		px+l
245	12.0	1800	5	B	C	ol+px+ga	ol+px+ga
242	12.0	1900	5	B	Mo	l	ga+l

A, simple cylindrical heater; B, sectioned (stepped) heater; C, graphite; Mo, molybdenum; ol, olivine; px, pyroxene; ga, garnet; l, quenched liquid.

* Thermocouple reading.

Figures 3*b*, 3*c*, and 3*d* show back scattered electron images of some of the run products. Quenched crystals always formed in the liquid portions of the samples.

Phase Relations

The phase relations of the two komatiites are shown in Figure 5. The liquidus temperature is slightly lower for Al-undepleted komatiite (AUK) than for Al-depleted komatiite and increases from about 1750°C at 4 GPa to about 1900°C at 12 GPa. For both of the compositions the liquidus phases are olivine in the lowest pressure range and garnet in the highest pressure range. The olivine liquidus interval is more extensive in the magnesium-rich ADK (up to 9.6 GPa) than in the AUK (up to 5.6 GPa). For the ADK pyroxene is the liquidus phase in an intermediate pressure range between 9.6 and 11.6 GPa, and for the AUK pyroxene appears at or very close to the liquidus near the 5.6 GPa olivine + garnet ± pyroxene multiple saturation point. Otherwise, clinopyroxene is the second phase to crystallize below the liquidus, and the third phase is garnet at low pressure and olivine at high pressure. The liquidus-solidus interval decreases from 150°C at 4 GPa to 75°C at 12 GPa. Local minima for this interval are reached at the olivine-pyroxene and pyroxene-garnet cosaturation points for the ADK and at the olivine-pyroxene-garnet multiple saturation point for the AUK.

Liquidus Phase Compositions

In order to evaluate the mineral-melt interaction related to partial melting or fractional crystallization of komatiites, we tried to obtain representative analyses of the minerals that crystallized in equilibrium with a liquid of composition identical or very similar to the bulk komatiite. Reconnaissance analyses of the 100% quenched liquid portions (hot zones) of some of the experimental charges of different run durations were performed in order to investigate whether the bulk composition is maintained within each segment of the charges. The small-scale inhomogeneous quench texture required raster type analyses covering areas of about 100 μm^2. These analyses indicate that there was no significant mass transportation of the type suggested by *Walker et al.* [1988] and *Lesher and Walker* [1988] along the axial thermal gradient in the furnaces within the run durations used in this study. Based on this observation, we analyzed the liquidus phases that are located at the border to the 100% liquid portions of the charges and in particular the crystals that are isolated from other crystals by intervening quenched liquid (e.g., Figure 3*d*).

The olivine compositions are given in Table 3. The forsterite contents of liquidus olivines in different run products range from 87.5 to 92.0 and increase as pressure increases. The K_d(Fe/Mg) values of the olivines in equilibrium with a liquid of bulk komatiite composition also increases slightly as a function of increasing pressure, except for two of the analyses (HSS-15, 138 and 135) with K_d values of about 0.6. The other

TABLE 3. Microprobe Analyses of Liquidus Olivines

Sample	M620	M620	HSS-15	HSS-15	HSS-15	HSS-15	HSS-15
Run #	138	260	138	135	168	156	247
p, GPa	4	5.5	4	5	6	7	10
T, °C	1700	1780	1700	1770	1800	1830	1860
SiO_2	39.4 (0.2)	40.0 (0.3)	39.3 (0.1)	40.4 (0.1)	41.2 (0.3)	40.9 (1.3)	40.9 (0.5)
Al_2O_3	0.16 (0.01)	0.83 (0.13)	0.14 (0.04)	0.23 (0.04)	0.12 (0.03)	0.17 (0.17)	0.82 (0.13)
FeO*	10.2 (0.1)	9.97 (1.21)	10.9 (0.1)	10.0 (0.01)	7.15 (0.15)	7.82 (0.14)	9.97 (0.57)
MnO	0.12 (0.02)	0.11 (0.04)	0.17 (0.01)	0.13 (0.02)	0.11 (0.02)	0.12 (0.02)	0.15 (0.03)
MgO	49.0 (0.1)	49.2 (0.7)	47.3 (0.1)	49.2 (0.1)	52.6 (0.2)	51.0 (1.0)	47.6 (0.1)
CaO	0.33 (0.01)	0.31 (0.14)	0.35 (0.02)	0.33 (0.01)	0.22 (0.01)	0.33 (0.14)	0.78 (0.38)
Total	99.2	100.4	98.2	100.3	101.4	100.3	100.2
Fo	89.4	89.7	88.4	89.6	92.8	92.0	89.3
K_d	0.41	0.40	0.65	0.57	0.38	0.43	0.59
			Cations Normalized to 4 Oxygen Atoms				
Si	0.978	0.979	0.988	0.983	0.986	0.990	0.999
Al	0.005	0.002	0.007	0.004	0.003	0.005	0.002
Fe	0.212	0.204	0.205	0.249	0.143	0.158	0.204
Mn	0.003	0.002	0.003	0.004	0.002	0.003	0.003
Mg	1.813	1.791	1.796	1.764	1.873	1.842	1.735
Ca	0.009	0.008	0.009	0.009	0.006	0.009	0.020
Total	3.020	2.986	3.008	3.013	3.013	3.007	2.963

Fo=[Mg/(Fe(t)+Mn+Mg)]*100; K_d=(FeO(t)/MgO)^{olivine}/(FeO(t)/MgO)$^{bulk\ komatiite}$. Oxides are in weight percent. Numbers in parantheses represent the uncertainty of analyses.

* Total iron as FeO

K_d values as well as the observed increase with increasing pressure are in accordance with the results by *Ulmer* [1989] and *Takahashi and Kushiro* [1983].

The pyroxene and garnet compositions are listed in Table 4. The calcium contents of the pyroxenes of different run products are quite variable. Subcalcic clinopyroxenes with 5-10 wt % CaO and highly variable aluminum contents predominate. Some of the pyroxenes, however, have less than 3 wt% CaO (e. g. the analysis from run product 138, Table 4) and may be orthopyroxenes. The moderate slope of the clinopyroxene limb of the diopside-enstatite solvus curvs [e.g., *Nickel and Brey*, 1984] results in considerable variation in the CaO-content of the clinopyroxene within a relatively small temperature range. The convergence of the coexisting clinopyroxene and orthopyroxene compositions with increasing temperature makes it difficult to establish whether two separate pyroxenes coexist in equilibrium or whether the compositional variation merely occurs within the clinopyroxenes. *Herzberg et al.* [this issue] found that orthopyroxene appearing in the 5-10 GPa pressure range in enstatite-rich compositions in the CMAS system is involved in the following peritectic relationship: orthopyroxene + melt = olivine + clinopyroxene + garnet.

The partition coefficient for Al (D_{Al}) between clinopyroxene and komatiitic liquid seems to decrease slightly with increasing pressure in the 4 to 11 GPa range. This is in accordance with the results of *Takahashi* [1986] and *Scarfe and Takahashi* [1986], who found a pronounced decrease in the aluminum content of clinopyroxene with increasing pressure. In contrast, the D_{Ca} between clinopyroxene and komatiite increases from 0.5 to 1.7 with increasing pressure.

Unlike the large liquidus olivine (20-80 mm) and clinopyroxene (10-40 mm) crystals, the garnets are generally small (less than 15 mm) and rounded. The liquidus garnets are pyrope dominated, and they contain a significant pyroxene component. The term majorite should not be used for these garnets, however, because the pyroxene component of the garnets does not exceed 10 mol %, and because the garnets coexist with pyroxene.

DISCUSSION

If the investigated AUK and ADK compositions are representative of near primary magmas, the liquidus phases shown in Table 2 and Figure 5 constrain the residual mineralogy and depth of magma separation from the source.

The Earth's mantle is dominantly peridotitic above the 400-km discontinuity [*Ringwood*, 1975; *Anderson*, 1989], and the volumetrically most important phases down to about 100 km depth are olivine and low calcium orthopyroxene. In the 100-400 km depth range, however, the abundances of clinopyroxene and garnet increase at the expense of orthopyroxene, and olivine remains the dominant phase [*Ito and Takahashi*, 1987]. Beacause of the increased solubility of the enstatite component in clinopyroxene and garnet with increasing temperature and pressure, respectively [*Nickel and Brey*, 1984; *Yamada and Takahashi*, 1984; *Kanzaki*, 1987], the mineral assemblages of some peridotites are reduced to olivine, garnet and clinopyroxene at solidus conditions above 3-5 GPa [*Takahashi*, 1986; *Scarfe and Takahashi*, 1986]. This assemblage is consistent with the low abundance or absence of orthopyroxene, the significant enstatite component of the liquidus garnets, and the subcalcic nature of the clinopyroxenes in our experiments.

Melting experiments using peridotitic and chondritic compositions show that olivine is the liquidus phase up to 11-16 GPa [*Takahashi*, 1986; *Ito and Takahashi*, 1987; *Ohtani et al.*, 1986; *Herzberg et al.*, this issue]. A large degree of partial melting with olivine as the only residual phase is therefore possible, and has been suggested as a mechanism to generate

TABLE 4. Microprobe Analyses of Liquidus Pyroxenes and Garnets

Sample	M620	HSS-15	HSS-15	HSS-15	M620	HSS-15
Run #	260	138	247	275	247	242
p, GPa	5.5	4	10	11	10	12
T, °C	1780	1700	1860	1875	1860	1900
SiO_2	52.7 (0.2)	54.2 (0.3)	55.3 (0.4)	57.5 (0.3)	43.5 (0.4)	45.5 (0.6)
TiO_2	0.16 (0.01)	0.06 (0.01)	0.08 (0.03)	0.02 (0.01)	0.25 (0.03)	0.14 (0.02)
Al_2O_3	5.68 (0.12)	2.46 (0.11)	1.43 (0.52)	2.25 (0.55)	21.7 (0.2)	20.2 (0.2)
FeO*	7.95 (0.33)	7.63 (0.09)	7.14 (0.35)	3.74 (0.16)	5.90 (0.12)	5.13 (0.17)
MnO	0.16 (0.01)	0.15 (0.02)	0.18 (0.03)	0.15 (0.02)	0.19 (0.02)	0.16 (0.01)
MgO	26.8 (0.8)	32.7 (0.2)	26.1 (0.7)	30.8 (0.9)	23.8 (0.4)	25.1 (0.4)
CaO	6.75 (0.21)	2.56 (0.02)	9.82 (0.64)	6.58 (0.12)	4.13 (0.17)	4.29 (0.09)
Na_2O	0.03 (0.01)	0.04 (0.01)	0.27 (0.03)	0.23 (0.02)		
Total	100.2	99.8	100.3	101.2	99.4	100.5
	Pyroxene Formulas Normalized to 6 Oxygen Atoms				Garnets Normalized to 12 Oxygens	
Si	1.864	1.904	1.963	1.966	3.057	3.150
Ti	0.004	0.002	0.002	0.001	0.013	0.007
Al	0.237	0.102	0.060	0.091	1.798	1.648
Fe	0.235	0.224	0.212	0.107	0.347	0.297
Mn	0.005	0.005	0.005	0.004	0.011	0.009
Mg	1.413	1.708	1.380	1.570	2.493	2.590
Ca	0.256	0.096	0.374	0.241	0.311	0.318
Na	0.002	0.003	0.019	0.015		
Total	4.016	4.044	4.015	3.995	8.030	8.019
En	74.2	84.2	70.2	81.9	Py 79.1	80.8
Fs	12.3	11.1	11.8	5.6	Alm 11.0	9.3
Wo	13.5	4.7	19.0	12.5	Gr 9.9	9.9
D_{Al}	0.71	0.72	0.42	0.66	2.73	5.91
D_{Ca}	0.89	0.45	1.73	1.16	0.54	0.76

$D_{Al}=(Al_2O_3)^{liquidus\ phase}/(Al_2O_3)^{bulk\ komatiite}$; $D_{Ca}=(CaO)^{liquidus\ phase}/(CaO)^{bulk\ komatiite}$; En, enstatite; Fs, ferrosilite; Wo, wollastonite; Py, pyrope; Alm, almandine; Gr, grossular. Oxides are in weight percent. Numbers in parantheses represent uncertainty of analyses.

* Total iron as FeO

komatiite magmas [*Green*, 1975]. However, the large thermal perturbations required for this process, combined with the low melt viscosities [see *Arndt*, 1977], does not support this scenario.

The compositional variation of various Al-undepleted and Al-depleted komatiites points to olivine and/or clinopyroxene control during melting or later fractionation [*Cawthorn and Strong*, 1974; *Bickle et al.*, 1977; *Nesbitt et al.*, 1979; *Smith and Erlank*, 1982]. In Figure 1, the mineral compositions of our experimental liquidus phases are plotted along with the compositions of representative komatiite samples in Al_2O_3 and CaO versus MgO variation diagrams. The liquidus olivine and clinopyroxene compositions (open squares and circles, respectively) plot close to the least squares linear regression lines for these komatiite compositions, whereas the garnet compositions (open triangles) deviate significantly from the lines.

The phase relations of the AUK (Figure 5) indicate that melt separation may have taken place at a pressure of about 5.6 GPa, leaving olivine, garnet, and pyroxene as residual phases. However, the relatively low Ca/Al and Ti/Al ratios of the AUK (Table 1) may be a result of nearly complete consumption of the residual garnet at an advanced melting stage.

According to the phase relations (Figure 5) the melting to form a primary magma of ADK composition progressed to a stage where either olivine or garnet was totally consumed by the melt. Melt separation most likely occurred at the pressure (depth) of one of the two liquidus cosatuaration points for the ADK (Figure 5), corresponding to the olivine-pyroxene cotectic at 9.6 GPa or the pyroxene-garnet cotectic at 11.6 GPa (Figure 6). Mantle peridotite compositions invariably have higher normative olivine contents than the pseudoinvariant melt composition at 9.6 GPa (Figure 6). Olivine will therefore remain as the major residual phase throughout the melting range of peridotites at this pressure, and garnet will be the first residual phase to disappear.

However, the chemical characteristics of the ADK (Table 1 and Figure 1) indicate that garnet was a residual phase at the time of melt separation, or that the source underwent premelting or synmelting garnet fractionation, e.g., from a rising peridotite diapir [*Green*, 1975; *Ohtani*, 1984]. In the latter scenario, garnet is gradually segregated from the upper portion of partially molten peridotite diapirs. Garnet is significantly denser than olivine and pyroxene (about 3.7 g/cm^3 versus 3.3-3.4 g/cm^3 at 10 GPa [*Ohtani*, 1984, 1988]) and is probably also denser than ultrabasic silicate liquids in the 10-15 GPa pressure range. The density of olivine may be similar to or slightly lower than that of the interstitial melt at these pressures [*Herzberg*, 1987*a*, *b*; *Agee and Walker*, 1988]. Such density relations will favor relative sinking of garnet crystals in a rising diapir containing a small melt fraction. When the melt fraction in the top of the diapir is sufficient for

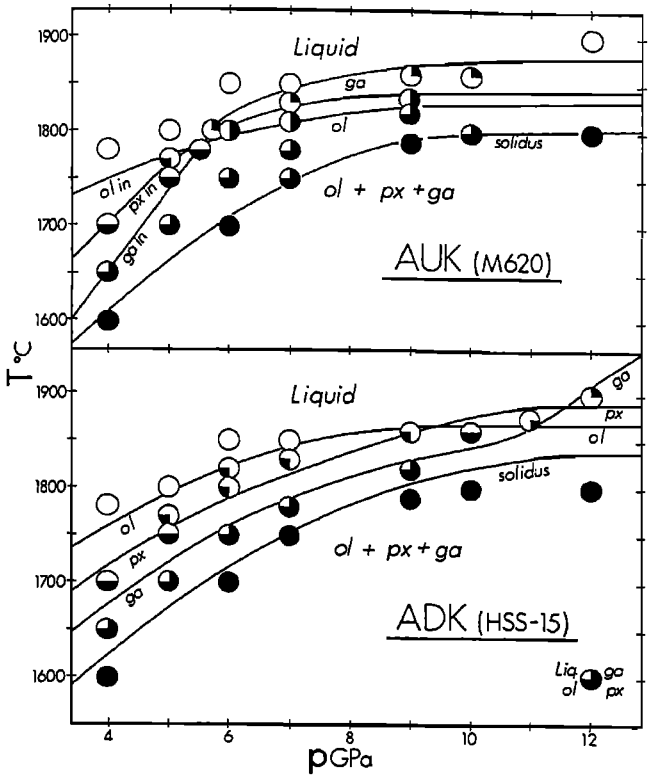

Fig. 5. Phase diagrams of the Al-undepleted (AUK) and Al-depleted (ADK) komatiites (samples M620 and HSS-15, respectively). The curved lines indicate the disappearance of the phases olivine (ol), pyroxene (px) and garnet (ga) with increasing temperature and melt fraction.

melt extraction, the liquid composition may be buffered by an olivine-clinopyroxene residue and have a garnet-depleted geochemical signature (i.e., low Al, HREE).

An alternative to the premelting or synmelting garnet fractionation is separation of the primary ADK melt from a garnet-pyroxene residue at a pressure of 11.6 GPa. This requires total consumption of the residual olivine during the partial melting, and this is possible only if the original source had less normative olivine than the pseudoinvariant melt composition at 11.6 GPa. The upper left hand portion of the mantle peridotite compositional field satisfies this requirement (Figure 6). Depletion of residual olivine could also occur in less fertile (higher normative olivine) peridotite source compositions during partial melting at pressures higher than 11.6 GPa. Partial melting of peridotite diapirs rising from 400 to 350 km depth (14 to 12 GPa pressure) could lead to segregation by sinking of melt that was more magnesian than the solid residue [*Herzberg*, 1987*a*, *b*; *Agee and Walker*, 1988]. Further melting of such a magnesium depleted residue along the pyroxene-garnet cotectic could produce the ADK.

Conclusions

The main differences between the investigated AUK and ADK compositions are their MgO and Al_2O_3 contents. Olivine is the liquidus phase up to 5.6 GPa in the AUK and 9.6 GPa in the Mg-rich ADK. The AUK has a multiple liquidus saturation point (olivine, pyroxene, and garnet) at 5.6 GPa, and a primary melt of AUK composition may have been separated from the three-phase residue at this pressure. The low Ca/Al ratio of this komatiite, however, indicates nearly complete melting of the residual garnet before melt separation.

The appearance of a 2-GPa pressure interval of liquidus pyroxene between the olivine and the garnet liquidus portions for the ADK points to more extensive melting and complete consumption of either garnet or olivine prior to the separation of primary melt of ADK composition. The high Ca/Al ratio of the ADK indicates either that garnet was a residual phase and that the partial melting proceeded along the garnet-pyroxene cotectic or into the garnet liquidus field or that garnet fractionation from the source preceded melt separation along the olivine-pyroxene cotectic at 9.6 GPa.

Consumption of the residual olivine is possible during partial melting of fertile peridotites above about 11 GPa, since the pseudoinvariant melt compositions are enriched in MgO relative to many fertile peridotites. Total melt consumption of olivine would occur more rapidly if the source was a peridotite-eclogite mixture. An alternative mode of formation of a primary magma of ADK composition is melt separation from a residue of olivine and pyroxene. The high Ca/Al ratio could then be ascribed to premelting or synmelting garnet fractionation from a partial molten peridotite diapir.

Assuming that the investigated AUK and ADK compositions represent near primary magma the depths of melt separation were probably about 150 km and 300-350 km,

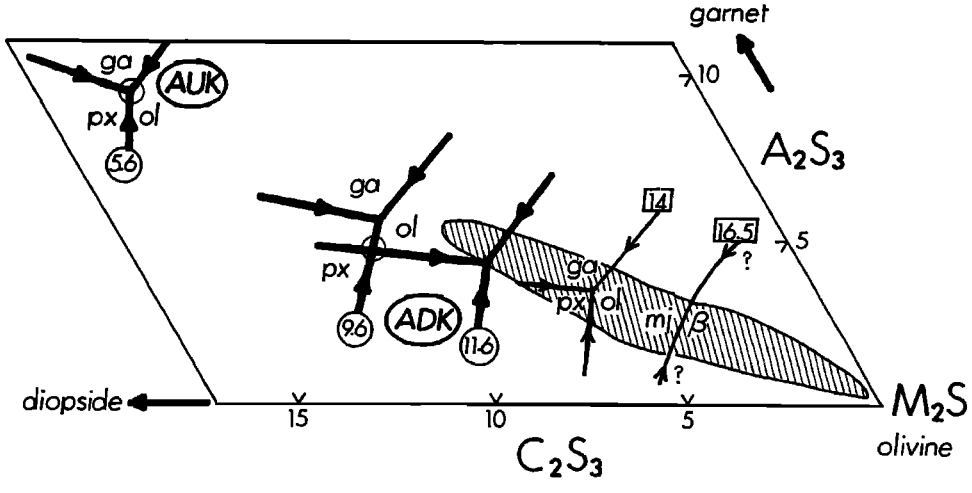

Fig. 6. Projection from enstatite (MS) into a portion of the plane M_2S-C_2S_3-A_2S_3 in the pseudoquaternary system CaO-MgO-Al_2O_3-SiO_2 (CMAS). The projection method is that of *O'Hara* [1968]. The composition of AUK (M620) and ADK (HSS-15) are given by circles. Tentative and approximate liquidus phase boundaries (numbers indicate pressure in gigapascals) are based partly on this study (heavy lines) and are drawn in approximate accordance with *Herzberg and Ohtani* [1988] and *Herzberg et al.* [this issue]. The stippled area is the field of mantle peridotite compositions [*Herzberg et al.*, this issue]. ga, garnet; py, pyroxene; ol, olivine; mj, majorite; β, β spinel.

respectively. The separation of the ADK magma followed either garnet fractionation and complete melt consumption of any remaining residual garnet, or complete melt consumption of olivine.

Acknowledgments. N. T. Arndt, Max-Planck-Institut für Chemie, Mainz, and H. S. Smith, University of Cape Town kindly provided the samples used as starting materials. We are thankful to Eiichi Takahashi for introducing us to the multianvil press technology and for valuable project suggestions. Claude Herzberg contributed greatly to the data interpretation throughout the study and provided preprints. Suggestions by D. Canil and D. C. Presnall; reviews by N. T. Arndt, T. Fujii, M. Kanzaki, and R. W. Luth; and technical assistance by D. Caird, J. Machacek, D. Tomlinson and P. Wagner are greatly appreciated. The study was financially supported by the Natural Sciences and Engineering Research Council of Canada grants SMI-105, CII0006947 and OGP0008394 to C.M.S. and OGP0041766 to R.G.T.

REFERENCES

Agee, C. B., and D. Walker, Static composition and olivine flotation in ultrabasic liquid, *J. Geophys. Res., 93*, 3437-3449, 1988.

Albee, A. L., and L. Ray, Correction factors for electron microprobe micro analyses of silicates, oxides, carbonates, phosphates and sulfates, *Anal. Chem., 42*, 1408-1414, 1970.

Anders, E., and N. Grevesse, Abundances of the elements: meteoric and solar, *Geochim. Cosmochim. Acta, 53*, 197-214, 1989.

Anderson, D. L., *Theory of the Earth*, Blackwell, Oxford, 1989.

Anhaeusser, C. R., The evolution of the early precambrian crust of the Southern Africa, *Philos. Trans. R. Soc. London, Ser. A, 273*, 359-388, 1973.

Anhaeusser, C. R., The geological evolution of primitive earth-evidence from the Barberton Mountain Land, in *Evolution of the Earth's Crust*, edited by D. H. Tarling, pp. 71-106, Academic, San Diego, Calif., 1978.

Anhaeusser, C. R., C. Riering, M. J. Viljoen, and R. P. Viljoen, The Barberton Mountain Land: a model of the elements and evolution of an Archaean fold belt, *Trans. Geol. Soc. S. Afr., 71*, annex, 225-253, 1968.

Arndt, N. T., Melting relations of ultramafic lavas (komatiites) at 1 atm and high pressure, *Year Book Carnegie Inst. Washington, 75*, 555-562, 1976.

Arndt, N. T., Ultrabasic magmas and high-degree melting of the mantle, *Contrib. Mineral. Petrol., 64*, 205-221, 1977.

Arndt, N. T., The field characteristics and petrology of Archean and proterozoic komatiites, *Can. Mineral., 17*, 147-163, 1979.

Arndt, N. T., and R. W. Nesbitt, Geochemistry of Munro Township basalts, in *Komatiites*, edited by N. T. Arndt and E. G. Nisbet, pp. 309-330, George Allen and Unwin, London, 1982.

Arndt, N. T., and R. W. Nesbitt, Magma mixing in komatiitic lavas from Munro Township, Ontario, in *Archaean Geochemistry*, edited by Kröner et al., pp. 99-114, Springer-Verlag, 1984.

Arndt, N. T., A. J. Naldrett, and D. R. Pyke, Komatiitic and iron-rich tholeiitic lavas in Munro Township, northeast Ontario, *J. Petrol., 18*, 319-369, 1977.

Arth, J. G., N. T. Arndt, and A. J. Naldrett, Genesis of Archean komatiites from Munro Township, Ontario: Trace element evidence, *Geology, 5*, 590-594, 1977.

Bence, A. E., and A. L. Albee, Empirical correction factors for the electron microanalysis of silicates and oxides, *J. Geol., 76*, 382-403, 1968.

Bickle, M. J., C. E. Ford, and E. G. Nisbet, The petrogenesis of peridotitic komatiites: Evidence from high-pressure melting experiments, *Earth Planet. Sci. Lett., 37*, 97-106, 1977.

Boyd, F. R., and J. L. England, The quartz-coesite transition, *J. Geophys. Res., 65*, 749-756, 1960.

Cattell, A., and N. T. Arndt, Low- and high-alumina komatiites from a late Archaean sequence, Newton Township, Ontario, *Contrib. Mineral. Petrol., 97*, 218-227, 1987.

Cawthorn, R. G., and D. F. Strong, The petrogenesis of komatiites and related rocks as evidence for a layered upper mantle, *Earth Planet. Sci. Lett., 23*, 369-375, 1974.

Fujii, T., M. Tachikara, and K. Kurita, Melting experiments in the system CaO-MgO-Al_2O_3-SiO_2 to 8 GPa: constraints on the origin of komatiites, *Eos Trans. AGU, 70*, 483, 1989.

Getting, I. C., and G. C. Kennedy, Effect of pressure on the emf of chromel-alumel and platinum-platinum 10%rhodium thermocouples, *J. Appl. Phys., 41*, 4552-4562, 1970.

Green, D. H., Genesis of Archaean peridotitic magma and constraints on Archaean geothermal gradients and tectonics, *Geology , 3*, 15-18, 1975.

Green, D. H., I. A. Nicholls, M. J. Viljoen, and R. P. Viljoen, Experimental demonstration of the existence of peridotitic liquids in earliest Archaean magmatism, *Geology , 3*, 11-15, 1975.

Hall, H. T., Fixed points near room temperature, in Accurate Characterization of the High-Pressure Environment, edited by E. C. Lloyd, *NBS Spec. Publ. 326*, 313-314, 1971.

Hamilton, P. J., N. M. Evensen, R. K. O'Nions, H. S. Smith, and A. J. Erlank, Sm-Nd dating of Onverwacht group volcanics, southern Africa, *Nature, 279*, 298-300, 1979.

Herzberg, C. T., Magma density at high pressure, part 1, The effect of composition on the elastic properties of silicate liquids, in Magmatic Processes: Physiochemical Principles, edited by B. O. Mysen, *Spec. Publ. Geochem. Soc., 1*, 25-46, 1987a.

Herzberg, C. T., Magma density at high pressure, part 2: A test of the olivine flotation hypothesis, in Magmatic Processes: Physiochemical Principles, edited by B. O. Mysen, *Spec. Publ. Geochem. Soc., 1*, 47-58,1987b.

Herzberg, C. T., and M. J. O'Hara, Origin of mantle peridotite and komatiite by partial melting, *Geophys. Res. Lett., 12*, 541-544, 1985.

Herzberg, C. T., and E. Ohtani, Origin of komatiite at high pressures, *Earth Planet. Sci. Lett., 88*, 321-329, 1988.

Herzberg, C. T., T. Gasparik, and H. Sawamoto, Origin of mantle peridotite: Constraints from melting experiments to 16.5 GPa, *J. Geophys. Res.*, this issue.

Homan, C. G., Phase diagram of Bi up to 140 kbars, *J. Phys. Chem. Solids, 36*, 1249-1254, 1975.

Ito, E., and E. Takahashi, Ultrahigh-pressure phase transformations and the constitution of deep mantle, in *High-Pressure Research in Mineral Physics, Geophys. Monogr. Ser.*, vol. 39, edited by M. H. Manghnani and Y. Syono, pp. 221-229, AGU, Washington, D.C., 1987.

Ito, E., E. Takahashi, and Y. Matsui, The mineralogy and chemistry of the lower mantle: An implication of the ultrahigh-pressure phase relations in the system MgO-FeO-SiO_2, *Earth Planet. Sci. Lett., 67*, 238-248, 1984.

Jahn, B. M., B. Auvray, S. Blais, R. Capdevila, J. Cornichet, F. Vidal, and J. Hameurt, Trace element geochemistry and petrogenesis of Finnish greenstone belts, *J. Petrol., 21*, 201-204, 1980.

Jahn, B. M., G. Gruau, and A. Y. Glikson, Komatiites of the Onverwacht Group, S. Africa: REE geochemistry, Sm/Nd age and mantle evolution, *Contrib. Mineral. Petrol., 80*, 25-40, 1982.

Kanzaki, M., Ultrahigh-pressure phase relations in the system $Mg_4Si_4O_{12}$-$Mg_3Al_2Si_3O_{12}$, *Phys. Earth Planet. Inter., 49,* 168-175, 1987.

Kushiro, I., A new furnace assembly with a small temperature gradient in solid-media, high-pressure apparatus, *Year Book Carnegie Inst. Washington, 75,* 832-833, 1976.

Lesher, C. E., and D. Walker, Cumulate compaction and melt migration in a temperature gradient, *J. Geophys. Res., 93,* 10,295-10,311, 1988.

Mirwald, P. W., and H. J. Massonne, The low-high quartz and quartz-coesite transition to 40 kbar between 600°C and 1600°C and some reconnaissance data on the effect of NaAlO2 component on the low quartz-coesite transition, *J. Geophys. Res., 85,* 6983-6990, 1980.

Nesbitt, R. W., S. S. Sun, and A. C. Purvis, Komatiites: Geochemistry and genesis, *Can. Mineral., 17,* 165-186, 1979.

Nesbitt, R. W., B. M. Jahn, and A. C. Purvis, Komatiites: An early precambrian phenomenon, *J. Volcanol. Geotherm. Res., 14,* 31-45, 1982.

Nickel, K. G., and G. Brey, Subsolidus orthopyroxene-clinopyroxene systematics in the system CaO-MgO-SiO2 to 60 kb: A reevaluation of the regular solution model, *Contrib. Mineral. Petrol., 87,* 35-42, 1984.

Nickel, K. G., G. P. Brey, and L. Kogarko, Orthopyroxene-clinopyroxene equilibira in the system CaO-MgO-Al_2O_3-SiO_2 (CMAS): New experimental results and implications for two-pyroxene thermometry, *Contrib. Mineral. Petrol., 91,* 44-53, 1985.

Nisbet, E. G., N. T. Arndt, M. J. Bickle, W. E. Cameron, C. Chauvel, M. Cheadle, E. Hegner, T. K. Kyser, A. Martin, R. Renner, and E. Roedder, Uniquely fresh 2.7 Ga komatiites from the Belingwe greenstone belt, Zimbabwe, *Geology, 15,* 1147-1150, 1987.

O'Hara, M. J., The bearing of phase equilibria studies in synthetic and natural systems on the origin and evolution of basic and ultrabasic rocks, *Earth Sci. Rev., 4,* 69-133, 1968.

Ohtani, E., Generation of komatiite magma and gravitational differentiation in the deep upper mantle, *Earth Planet. Sci. Lett., 67,* 261-272, 1984.

Ohtani, E., Chemical stratification of the mantle formed by melting in the early stage of the terrestrial evolution, *Tectonophysics, 154,* 201-210, 1988.

Ohtani, E., T. Kato, and H. Sawamoto, Melting of a model chondritic mantle to 20 GPa, *Nature, 322,* 352-353, 1986.

Pyke, D. R., A. J. Naldrett, and O. R. Eckstrand, Archean ultramafic flows in Munro Township, Ontario, *Geol. Soc. Am. Bull., 84,* 955-978, 1973.

Ringwood, A. E., Mineralogy of the mantle, in *Advances in Earth Sciences,* edited by P. M. Hurley, pp. 357-399, MIT Press, Cambridge, Mass., 1966.

Ringwood, A. E., *Composition and Petrology of the Earth's mantle,* 618 pp., McGraw-Hill, New York, 1975.

Scarfe, C. M., and E. Takahashi, Melting of garnet peridotite to 13 GPa and the early history of the upper mantle, *Nature, 322,* 354-356, 1986.

Smith, H. S., and A. J. Erlank, Geochemistry and petrogenesis of komatiites from the Barberton greenstone belt, South Africa, in *Komatiites,* edited by N. T. Arndt and E. G. Nisbet, pp 347-397, George Allen and Unwin, London, 1982.

Suito, K., Phase relation of pure Mg_2SiO_4 up to 200 kilobars, in *High Pressure Research-Application to Geophysics,* edited by M. H. Manghnani and S. Akimoto, pp. 255-266, Academic, San Diego, Calif., 1977.

Sun, S. S., and R. W. Nesbitt, Petrogenesis of Archean ultrabasic and basic volcanics: Evidence from rare earth elements, *Contrib. Mineral. Petrol., 65,* 301-325, 1978.

Takahashi, E., Melting of a dry peridotite KLB-1 up to 14 GPa: Implications on the origin of peridotitic upper mantle, *J. Geophys. Res., 91,* 9367-9382, 1986.

Takahashi, E., and I. Kushiro, Melting of a dry peridotite at high pressures and basalt magma genesis, *Am. Mineral., 68,* 859-879, 1983.

Takahashi, E., and C. M. Scarfe, Melting of peridotite to 14 GPa and genesis of komatiite, *Nature, 315,* 566-568, 1985.

Takahashi, E., H. Yamada, and E. Ito, An ultrahigh-pressure furnace assembly to 100 kbar and 1500 °C with minimum temperature uncertainty, *Geophys. Res. Lett., 9,* 805-807, 1982.

Ulmer, P., The dependence of the Fe^{2+}-Mg cation-partitioning between olivine and basaltic liquid on pressure, temperature and composition: an experimental study to 30 kbar, *Contrib. Mineral. Petrol., 101,* 261-273, 1989.

Viljoen M. J., and R. P. Viljoen, Evidence for the existence of mobile extrusive peridotitic magma from the Komati Formation of the Onverwacht group, *Spec. Publ. Geol. Soc. S. Afr., 2,* 87-112, 1969*a*.

Viljoen, M. J., and R. P. Viljoen, The geology and geochemistry of lower ultramafic unit of the Onverwacht group and a proposed new class of igneous rocks, *Spec. Publ. Geol. Soc. S. Afr., 2,* 55-86, 1969*b*.

Viljoen, R. P., and M. J. Viljoen, The effects of metamorphism and serpentinization on the volcanic and associated rocks of Barberton region, *Spec. Publ. Geol. Soc. S. Afr., 2,* 29-54, 1969*c*.

Viljoen, M. T., R. P. Viljoen, and T. N. Pearton, The nature and distribution of Archean komatiite volcanic in South Africa, in *Komatiites,* edited by N. T. Arndt and E. G. Nisbet, pp. 53-79, George Allen and Unwin, London, 1982.

Walker, D., S. Jurewicz, and E. B. Watson, Adcumulus dunite growth in a laboratory thermal gradient, *Contrib. Minral. Petrol., 99,* 306-319, 1988.

Williams, D. A. C., and R. G. Furnell, Reassessment of part of the Barberton type area, South Africa, *Precambrian Res., 9,* 325-347, 1979.

Yagi, T., M. Akaogi, M. Arashi, T. Okai, K. Kawamura, K. Shino, M. Shimomura, T. Suzuki, K. Tabata, and S. Akimoto, Precise determination of olivine-spinel phase transformation in Fe_2SiO_4, *J. Geophys. Res., 92,* 6207-6213, 1987.

Yamada, H., and E. Takahashi, Subsolids phase relations between coexisting garnet and two pyroxene at 50 to 100 kbar in the system CaO-MgO-Al_2O_3-SiO_2, in *Kimberlites II: The Mantle and Crust-Mantle Relationships,* edited by J. Kornprobst, pp. 247-255, Elsevier, New York, 1984.

Zindler, A., Nd and Sr isotopic studies of komatiites and related rocks, in *Komatiites,* edited by N. T. Arndt and E. G. Nisbet, pp. 399-421, George Allen and Unwin, London, 1982.

R.G. Trønnes and K. Wei, Department of Geology, University of Alberta, Edmonton, Canada T6G 2E3.

(Received July 24, 1989;
revised December 22, 1989;
accepted January 3, 1990.)